SMART-X,

"Square Meter, Arcsecond Resolution X-ray Telescope"

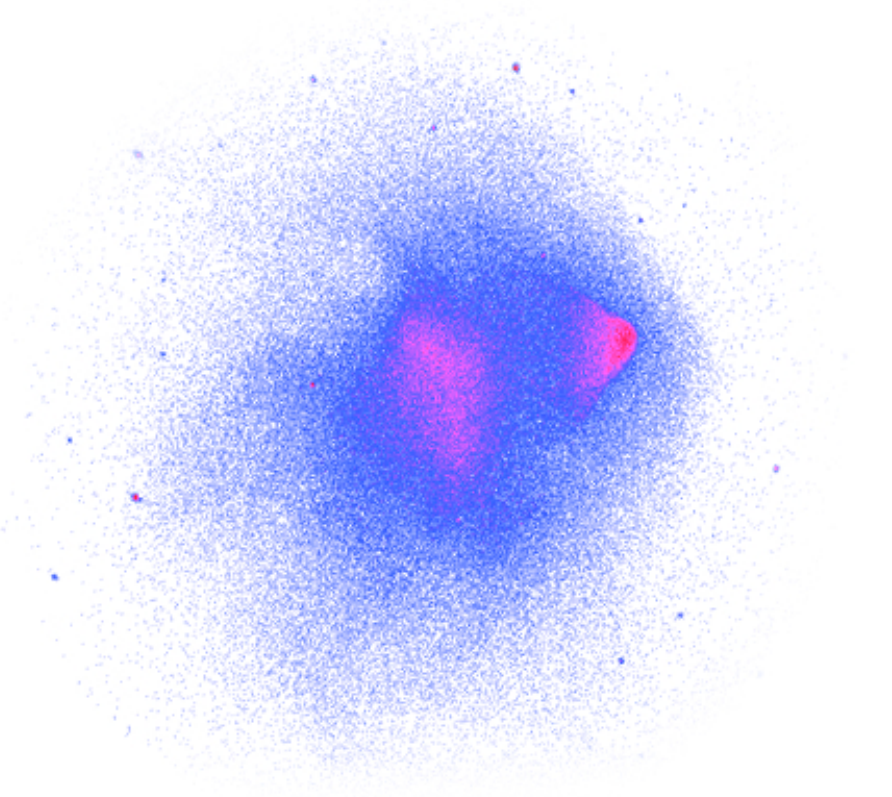

A mission concept for a 2.3 m^2 effective area, 0.5″ angular resolution X-ray telescope, with 5′ FOV, 1″ pixel size microcalorimeter, 22′ FOV imager, and high-througput gratings.

submitted by Alexey Vikhlinin
Smithsonian Astrophysical Observatory
617-495-7044, avikhlinin@cfa.harvard.edu

on behalf of the *SMART-X* team at
SAO, PSU, MIT, GSFC, MSFC, JHU, Stanford, U.Waterloo, Rutgers, NIST
in response to NNH11ZDA018L

A. Vikhlinin, P. Reid, H. Tananbaum, D. A. Schwartz, W. R. Forman, R. Kraft, C. Jones, J. Bookbinder, R. Smith, V. Controneo, A. Kenter, P. Nulsen, L. P. David, R. Brissenden (SAO)

S. Tolier-McKinstry, D. Burrows, A. Falcone, W. N. Brandt, E. Feigelson, L. Townsley (PSU)

M. W. Bautz, M. Schattenburg, R. Heilmann, J. Davis, D. Dewey (MIT)

S. R. Bandler, M. Markevitch, R. E. Kelley, C. A. Kilbourne, F. S. Porter, S. J. Smith (GSFC)

M. C. Weisskopf, B. Ramsey, S. O'Dell (MSFC)

S. S. Murray (JHU)

S. A. Allen (Stanford)

B. R. McNamara (U. Waterloo)

J. P. Hughes (Rutgers)

K. D. Irwin, G. C. Hilton (NIST/Boulder)

A. Vikhlinin and other members of the *SMART-X* team are willing to participate and present our concept at the workshop.

We are willing to discuss all information related to the proposal.

1 Overview

We describe the Square Meter Arcsecond Resolution X-ray Telescope — *SMART-X*— in response to this Request for Information for mission concepts capable of addressing scientific objectives of the International X-ray Observatory. We propose to leverage an emerging adjustable optics technology to build an even more scientifically ambitious mission, but more efficiently. Our *SMART-X* concept includes substantial simplifications and cost reductions relative to IXO — shorter focal length eliminating the extendable optical bench and reducing mass and structural complexity, fewer science instruments, and streamlined operations — and in this, it is similar to the AXSIO concept. Adding subarcsecond resolution, *SMART-X* will build upon Chandra's success and IXO's ambitions, becoming a major and indisputable scientific advance at an affordable cost. To generate sustained support, a mission concept should be able to capture the imagination of the scientific community, and *SMART-X* will do exactly that.

SMART-X will be capable of addressing almost all of the IXO science goals — growth of SMBH and strong gravity effects; evolution of large scale structure and detection of the WHIM; AGN feedback and cycles of matter and energy (even at high z, Fig. 1). In many areas, *SMART-X* transcends the scope of IXO. It will be able to carry out surveys to the *Chandra* deep fields depth over 10 deg^2; study galaxy assembly processes to $z = 2.5$; and track the evolution of group-sized objects, including those hosting the first quasars, to $z = 6$; open new opportunities in the time domain and high-resolution spectroscopy.

Over the past few years we have developed the concept of the adjustable-optic telescope. With some initial technical success, we now believe that it is timely to introduce this approach to the discussion of future directions in X-ray astronomy. The challenge is to develop the optics to a high level of technical readiness over the next several years to provide *Chandra*-like 0.5″ half-power diameter angular resolution with IXO-like area (2.3 m^2 at 1 keV or ≈ 30 times *Chandra*). This is a tremendous increase — recall that a factor of 4 increase in are from Palomar to Keck as considered a breakthrough at the time. With Keck, there were additional scientific gains from detector advances. For *SMART-X*, we also plan for advanced instruments: 1) an active pixel sensing imager for surveys, sub-arcsecond imaging, and soft-band response; 2) a 5′ × 5′ field of view microcalorimeter with 1″ pixels and 5 eV energy resolution; and 3) a high throughput X-ray grating spectrometer.

The *SMART-X* optics use slumped glass mirror segments with deposited piezoelectric actuators energized to correct mirror figure errors from 10″ (achieved for IXO) to $\lesssim$ 0.5″. This concept builds upon the mirror development for IXO, both in terms of the thermally formed substrates, as well as mirror alignment and mounting. Work on the optics technology is already underway, and we lay out a program for the current decade to reach TRL6 at an estimated cost of $45M.

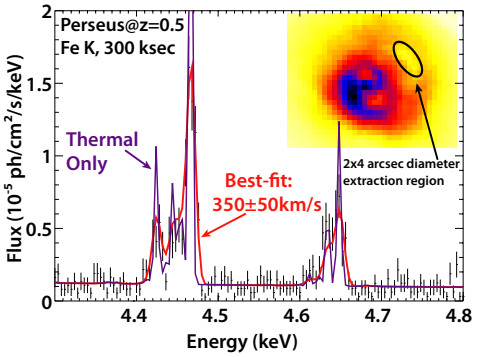

Fig. 1— *SMART-X*/XMIS observation of the Perseus cluster placed at $z = 0.5$. Statistics are sufficient to image the bubble structure around the central black hole and measure turbulence in a 2″ × 4″ region.

With funding for mission studies and technology in a few key areas during the current decade, *SMART-X* can be developed and launched in the 2020's. Our estimated end-to-end mission cost, based on current AXSIO work and taking into account the changes to transition to *SMART-X*, is $2,328M, slightly beyond the guidelines of this RFI.

We recognize that AXSIO represents major advances and is ready to start development within 2–3 years if the ATHENA mission is not selected by ESA. For the next few years, continued NASA support for AXSIO also will be directly applicable for a *SMART-X* mission. The AXSIO work along with focused technology investment for *SMART-X* enables a resilient and forward-looking X-ray astronomy program. Whether or not ATHENA or AXSIO proceeds in this decade, *SMART-X* is a qualitative leap forward and is the logical candidate for *the* major X-ray mission of the 2020's.

2 *SMART-X* Optics

Mirror Design. The *SMART-X* mirror design draws from previous IXO studies and uses slumped glass segments. The 3 m diameter aperture is covered with 292 shells forming a Wolter-type[1] mirror with a 10m focal length. Mirror segments are 200mm long with azimuthal spans ranging from 150 to 380mm. This model has been ray-traced assuming an Ir coating and accounting for structural obscurations, large angle scattering, contamination, and small alignment errors. Raytrace calculation gives an effective area of 2.3 m^2 at 1 keV (see Fig. 5 below) and shows that the blur due to off-axis aberrations from the Wolter-I design is within 0.5″ half power diameter out to 2.5′ off-axis. Losses in effective area due to shadowing and vignetting are less than 50% for all energies out to ~ 8.5′ off-axis. At 2 keV, loss of EA is < 20% within the inner 10′, providing a useful field of view of at least 20′ × 20′ for survey work

[1] Our present estimated are based on ray-trace modeling of a Wolter-1 telescope; we will also consider a Wolter-Schwarzschild and polynomial designs to improve the off-axis point response function.

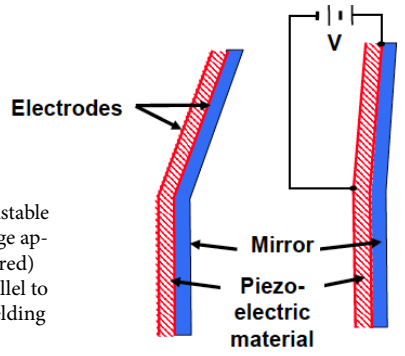

Fig. 2— Bimorph adjustable mirror concept. Voltage applied across the PZT (red) produces a strain parallel to the mirror surface, yielding a localized deflection.

and imaging of extended sources.

The mirror segments are made of either 400 µm thick thermally formed glass sheets (similar to those used in LCD displays), or 100–200 µm thick electroformed nickel/cobalt replicated mirror segments. The flight mirror assembly mass is estimated at 890 kg, where the mirror segments and support structure each contribute 50%.

Adjustable mirrors. Our approach to achieving 0.5″ angular resolution with segmented, lightweight mirrors is to make each individual segment adjustable. A ground electrode is deposited on the back of the mirror, then a thin (1–5 µm) layer of piezoelectric material (lead zirconate titanate, or PZT) is deposited on the ground electrode; and lastly, a "pixelated" array of independently addressable electrodes is deposited on the piezo material to form an array of piezo "cells". As a voltage is applied between the ground electrode and one of the back surface electrodes, strain in the piezo cell causes controllable local bending in the mirror (concept illustrated in Fig. 2). By controlling the voltage applied to each cell, the correction can be made to match the local figure errors in the mirror, correcting the thin mirror figure to a level not achievable by ordinary means. The appropriate voltage is applied to each cell for the duration of the mission. Nominal leakage current is only ~ 0.01 mA at 10 V, so operating power even for 10^6 adjusters is a few hundred watts.

We project that a mirror figure quality corresponding to 0.5″ angular resolution can be achieved by having the individual segments adjusted essentially once. Figure errors after mounting and alignment will be measured by optical surface metrology. These errors as well as deformations

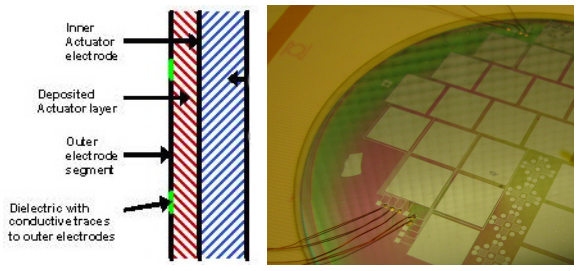

Fig. 3— *Left:* Cross-sectional schematic of the PZT cell structure. *Right:* A photo of a flat Corning Eagle™ test mirror with deposited PZT film and a pattern of the independently addressable electrodes.

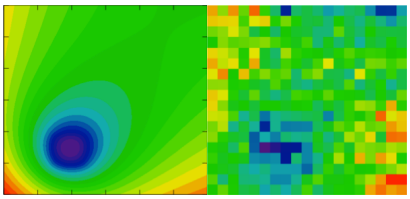

Fig. 4— Finite element modeling prediction (*left*) and measured deformation (*right*) in response to an individual cell activation in one of the first experiments.

due to gravity release and the nominal on-orbit thermal environment will be corrected by applying an optimal set of voltages to each mirror segment. Depending on mission safety requirements, the piezos can either be left energized through launch, or the power supplies turned off, and the piezos energized once on-orbit.

We believe that segmented mirrors are better suited for adjustment than full shells. In the latter, it is impossible to make localized corrections because of hoop stresses, and this greatly compromises the efficacy of figure control. In segmented mirrors, the corrections are more localized. The response to activation of each cell can be measured and modeled as a function of voltage, determining a set of influence functions. Determining the sets of piezo voltages required to correct the mirror figure then becomes a linear 2-dimensional matrix inversion problem.

Current state of technology. SAO and PSU working together have made significant progress with adjustable X-ray optics, and consider the technology to be at TRL2 and approaching 3[2]. Foremost, and for the first time to our knowledge, we have demonstrated the deposition of thin film piezoelectric material on test mirrors over cells as large as 1 cm^2 (Fig. 3) and the energizing of that piezo to produce a localized figure change consistent with expectations (Fig. 4). Piezo thickness, properties, and achieved strain (800 ppm) meet requirements dictated by starting with an ~ 10″ PSF for an uncorrected mirror pair and correcting it to < 0.5″.

Large deformations of the mirror substrate can occur during piezo deposition due to the 550C temperature required for successful deposition. We showed PZT can be deposited on Corning Eagle™ glass, which has a strain temperature ~ 130C higher than Schott D263™, the glass used by IXO. Piezo processing is now more than 100C below the glass strain temperature. Initial inspection shows no large deformations occurred during this process.

Investigations of mirror lifetime, stability, and repeatability have begun. We note that PZT has been used in space for focus control on the AIA telescopes on the Solar Dynamics Observatory [2], and also used in the Fine Guidance Sensors developed for JWST [3]. The thermal sensitivity of thin film PZT is very small, ~ 1% per degree C at nominal *SMART-X* mirror and laboratory temperatures, 20–21C [4]. Lifetime applied voltage cycling tests confirm

[2] Note also that a subset of this technology is already being used for 1-D correction of synchrotron X-ray optics [1].

that a required level of stability of the piezoelectric coefficient can be achieved over space mission lifetimes [5, 6].

We are developing a finite element analysis model for adjustable mirror segments to study strategies for correcting "generic" figure errors and develop optimization techniques. To date, we have modeled the impact of mounting constraints on the shape of the influence functions and demonstrated that the more over-constrained the mount, the more localized are the influence functions [7]. We also modeled gravity release to determine how well it could be corrected. We found that gravity release errors are small, $\sim 0.11''$ rms, and can be almost entirely removed by piezo actuators (to $\sim 0.01''$ rms, [8]).

High angular resolution can be achieved through piezo adjustment only if we start with segments with suitably small upper mid and high spatial frequency mirror figure errors. To minimize the introduction of these errors during slumping, we developed an approach using a sputtered, smooth platinum release layer for thermal forming, replacing the more typical rough, sprayed, boron nitride. We produced test samples and measured micro-roughness over spatial periods from 1 mm down to a few nm for several glasses — Schott D263™, AF45™, and Corning Eagle™. All showed comparable smoothness and roughness consistent with sub-arcsecond imaging (~ 4 Å, RMS).

Mirror technology development plan and cost. The technology roadmap and development plan focus on achieving TRL6 by 2020. The roadmap includes mirror [PZT] lifetime and yield, alignment and mounting, performance, extension from flat test mirrors to conical Wolter segments, and ultimately, demonstration of $0.5''$ imaging using a 2–3 shell mirror assembly in the zero-gravity environment of a sounding rocket.

Flat test mirrors will continue to be used for developing PZT film deposition. This includes experiments to increase yield[3] by optimizing the Pb content of the film. Excess Pb, which reduces yield, can also be removed by annealing the PZT film. The "high temperature" Corning Eagle™ glass enables greater use of annealing to optimize film composition. Mn and Nb doping have been shown to significantly improve piezo stability [9], and will be explored to increase lifetime.

To optimize the piezo mirror figure correction, we will: (1) study the optimal layout and shape of the electrode pattern (square, rectangular, or hexagonal, brickwork overlapping array, etc.); (2) experiment with non-uniform electric field within individual cells by changing the size of the electrode relative to that of the piezo cell, and by altering the shape of sub-sized electrodes; (3) test smaller piezo cells at the segment edges to better control edge effects.

Extending adjustable optics technology to Wolter-type mirror segments requires modifying the PZT deposition process and top surface electrode deposition for conical curved surfaces (both are relatively straightforward). Printing of the top electrode pattern can be accomplished either by shadow mask lithography or by direct electron beam writing. We believe that this area, as well as defining a mass production approach, is best developed through our planned partnership with the industry.

Optical metrology approaches similar to those developed for IXO can be followed for *SMART-X* because of the close mirror optical design. We can use either the *Chandra* approach of tying together axial interferometry data with azimuthal scans to build a full 2-d surface map, or the IXO approach of employing a cylindrical null corrector to obtain full surface metrology for each mirror segment [10]. We plan to demonstrate that the adjustable optic functions properly with a conical segment in CY2013.

Optical metrology and finite element modeling will play critical roles throughout the development. Models will be adjusted through comparison of their predictions with actual measurements, thus improving their use as a predictive tool. Optical metrology will make use of an optical interferometer (such as Zygo or 4D) which has sufficient accuracy to achieve better than $0.5''$ imaging, and an optical profilometer, which has less accuracy, but a larger surface dynamic range.

SMART-X mirror segments must be mounted and aligned to $< 0.25''$ (achieved on *Chandra* for 4 mirror pairs). Significant relevant technology development has already been done for Con-X/IXO/AXSIO, including two mounting approaches that are converging to meet AXSIO requirements. Compared to AXSIO, we can tolerate larger mounting distortions (up to a few arcsec) because these can be corrected by the piezos. On the other hand, the level of alignment achieved for AXSIO is insufficient for *SMART-X* and this will require further work. Thus *SMART-X* development will focus on using a more constrained mount (e.g., 12 support points vs. 6–10 for AXSIO), improved alignment accuracy, while allowing increased figure deformation during mounting. Only small improvements are required to the alignment metrology, already demonstrated to an accuracy of $\sim 0.25''$. Conceptual designs exist for the *SMART-X* alignment and mounting, but further development and demonstration is required.

Lifetime testing will be performed to confirm stability of the piezo electromechanical properties over a multi-year period and in a vacuum environment, and to further verify that its radiation resistance [11] meets the *SMART-X* needs. Preliminary lifetime tests will begin in FY12 at SAO, using strain gauges to monitor thin film PZT performance as a function of time and vacuum environment.

A more formal outline of the technology development program is as follows (see also Appendix B). To complete requirements for TRL3, it remains to improve the accu-

[3] At present, the yield (fraction of good piezo "cells") ranges from 40% to 96% depending upon deposition parameters and piezo annealing.

Table 1— *SMART-X* Science Instrument Capabilities

	Energy Band	Energy Resolution	Angular Resolution	Field of View
CATGS	0.2–1.2 keV	$E/\Delta E > 4000$	0.5″ across dispersion	...
APSI	0.2–8 keV	37 eV @ 0.3 keV, 120 eV @ 6 keV	0.5″ mirror, 0.33″ pixels	22′ × 22′
XMIS	0.2–10 keV	5 eV	1″ pixels	5′ × 5′
Mirror	0.1–10 keV	...	0.5″ on-axis, 0.7″ @ 2.5′, 4″ @ 10′	10′ radius

racy of adjustment shown in Fig. 4 to ±40Å and to verify sufficiently low levels of upper mid-frequency ripple and high-frequency micro-roughness on a conical mirror element with piezo actuators deposited. We plan to accomplish these tasks in the next 18 months. By 2015 we plan to demonstrate adjustment of curved elements to a precision consistent with 0.5″ imaging and develop a module for alignment of multiple shells to within 0.2″, reaching TRL4. By 2016, we will demonstrate TRL5 with a breadboard module of several mirror pair segments, with realistic connections to piezo drivers and alignment hardware, which will undergo environmental testing and measurement in an X-ray test beam. Technology will be in place for a rocket flight in 2017–2018, with a mirror assembly of 2–3 shells, to observe a bright source (e.g., Sco X-1). Demonstration of 0.5″ imaging performance in a space environment, while surviving launch, will result in achieving TRL6.

The estimated cost for this program is $45M in FY12 dollars. The cost schedule includes $2.8M for program management and $42.2M for eight major task groups: alignment and mounting ($9M, 2013–2015), optimizing influence function shape ($3.5M, 2013–2017), improving mid-frequency figure via thermal forming with Pt release layer ($2.2M, 2012–2015), PZT development ($4.25M, 2012–2015), metrology development ($2M, 2014–2016), extending the technology to conical mirrors, including X-ray testing ($14.7M, 2012–2018), sounding rocket program ($5M, 2013–2018), and lifetime testing ($1M, 2012–2019).

3 *SMART-X* Science Instruments

We envision three science instruments for *SMART-X*. The deployable Critical Angle Transmission Grating Spectrometer (CATGS) will provide a resolving power of $R > 4000$ with large collecting area across the 0.2–1.2 keV energy band. The two prime focus imaging instruments, on a movable translation stage, are complementary and provide some redundancy. The Active Pixel Sensor Imager (APSI) is optimized for high-resolution imaging, provides a large FOV (22′ × 22′) for surveys, and has excellent response at $E < 0.5$ keV for studies of high-redshift objects. The X-ray Microcalorimeter Imaging Spectrometer (XMIS) provides 5 eV spectroscopy and good high-E efficiency, while still maintaining 1″ imaging. The zeroth-order image in the prime focus can be taken using either APSI or XMIS.

3.1 Critical Angle Transmission Grating Spectrometer

The X-ray Grating Spectrometer (CATGS) provides high-resolution, very high-throughput spectroscopy in the 0.2–1.2 keV band. The CATGS consists of an array of Critical

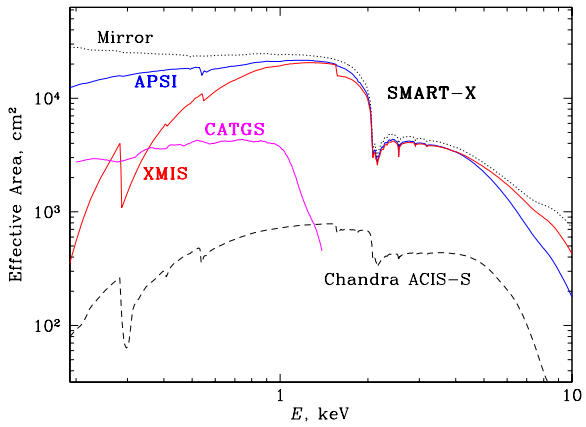

Fig. 5— Effective area of the *SMART-X* optics and science instruments.

Angle Transmission (CAT) gratings on a deployable mount located behind the flight mirror assembly, together with a dedicated readout subsystem on the *SMART-X* focal plane. The instrument architecture is similar to that of *Chandra*'s HETG, which was built by the CATGS team and which has been operating successfully for more than 12 years.

The CAT grating is a novel optical element [12] that combines the low mass and relaxed alignment and figure tolerances of a transmission grating with the excellent diffraction efficiency and resolving power of blazed reflection gratings used in high-diffraction order. CAT gratings are manufactured at MIT from silicon wafers using microfabrication techniques. The technical readiness of CAT gratings was evaluated during IXO definition studies and judged to be at TRL3 in 2009 on the basis of prototype grating performance measurements at a synchrotron radiation facility. A technology development plan was developed then and substantial progress on fabrication of grating support structures has been made in the past two years. We expect to achieve TRL4 in 2012. With adequate funding, we expect to reach TRL5 no later than 2015.

The sub-arcsecond angular resolution of the *SMART-X* mirror enables excellent dispersive spectral resolution without use of the sub-aperturing required for optics similar to IXO's. As a result, the CATGS gratings can be deployed over the entire mirror aperture for maximum effective area (for *SMART-X*, our baseline is to cover 50% of the aperture, constrained by cost), while using a single linear readout array which substantially reduces the complexity and cost of the instrument. Thus, *SMART-X*/CATGS exploits technologies developed for IXO to provide extraordinary improvements in spectral resolving power and

effective area. With a 3.0° blaze angle optimizing the trade-off between efficiency and the high-energy cutoff, CATGS will achieve a ***resolving power*** of $R > 4000$ across the 0.2–1.2 keV band and a 0.4 m^2 ***collecting area***.

The CATGS readout subsystem, CATGSR, is a linear array of Si-based active pixel sensors (§3.2 below), placed on a fixed platform ~ 60 cm off the primary focus on a separate focusing mechanism and aligned tangent to the Rowland torus. The energy resolution of the CATGS readout provides spectral order sorting. The 0-th order image can be provided by either the APSI or the XMIS arrays. Because the silicon CAT gratings are relatively thin (6 μm), the prime imaging focus retains significant effective area at $E > 1$ keV even with the gratings in the beam.

3.2 Active Pixel Sensor Imager. The *SMART-X* Active Pixel Sensor Imager (APSI) is an array of active pixel sensors tuned for high-resolution, wide-field imaging at the prime focus, and providing excellent soft-band sensitivity needed for observations of high-redshift sources. The same technology will be used for a separate array, CATGSR, needed for the readout of the dispersed CATGS spectra.

Si-based sensors based on CMOS technology already meet many of the *SMART-X* requirements. CMOS detectors have been developed along two primary lines: CMOS hybrids (e.g., the PSU/Teledyne [13] and the MIT three dimensional integrated circuit technology [14]), and monolithic CMOS (e.g., SAO/Sarnoff [15] and the MPI DEPFET [16]). Hybrid CMOS devices have deep depletion for good QE at high-E, they are four side abuttable for constructing large mosaics, but currently show high read noise, ~ 10 e^- and poor low energy resolution. Monolithic devices demonstrate low readnoise, < 2 e^-, good low-energy response, but currently have small depletion depth, < 20 μm, limiting QE above 2 keV.

Straightforward, achievable developments will ensure that all requirements, listed below, are met and TRL5 reached by 2020. We aim for a ***pixel size*** of 16 μm = 0.33″, smaller than the angular/dispersive resolution of the mirror. APSI is a > 16 megapixel array covering at least 22′×22′ FOV in the prime focus. We will work to reduce the pixel size to better oversample the PSF and increase the number of pixels to maintain a ~ 20′ FOV. CATGSR is a linear array with a total length of ~ 20 cm. Full-frame ***readout rates*** for both arrays are 100 s^{-1} to minimize dark current and optical load. A thin, 10–20 nm, layer of Al (achieved at PSU) capped with an Al_2O_3 layer of comparable thickness (under development at MIT) serves to block stray light from XUV to the near IR with minimal impact on soft X-ray response, resulting in high QE for the sensor+filter system down to $E \lesssim 0.2$ keV. Very optically bright sources can be observed with XMIS which has a thick filter. ***Energy resolution*** in both cameras is Fano-limited over the entire band. APSI will have high-speed ***windowing capability*** to avoid pileup and perform μs timing of bright sources.

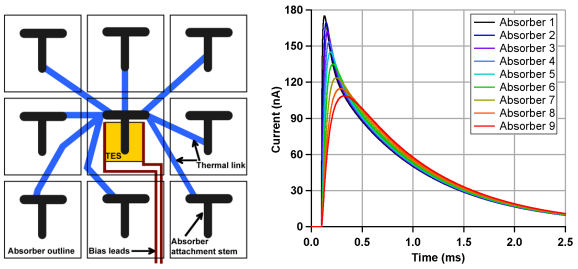

Fig. 6— *Left:* Schematic diagram of the Hydra concept, showing nine absorbers, each with a different thermal conductance, connected to a single TES. Each absorber is supported above the TES and solid substrate using small stem contact regions (shown as "T" shapes here). *Right:* Simulated 9-pixel Hydra noise-less pulse shapes for a photon energy of 100eV. Absorber 1 is the most strongly coupled absorber to the TES.

Devices will have sufficient radiation hardness to withstand the projected mission lifetime without significant degradation.

We note that there are important distinctions in the requirements for the APSI and CATGSR cameras. CATGSR does not require sensitivity above ~ 2 keV, but it needs high quantum efficiency and energy resolution down to the lowest possible energy (100 eV). The monolithic technology is a good match for both of these aspects of performance. For the APSI, the higher energy response is more required, while a higher readout noise can be tolerated. These aspects better match the performance of the hybrid detectors and the general direction of their technology developments. Therefore, while the goal is identical technology for both APSI and CATGSR, we note that the two cameras can at the very least be built using separate, monolithic and hybrid, sensors. The sensors are sufficiently similar so that nearly identical electronics packages can be used to drive and process the data.

3.3 X-ray Microcalorimeter Imaging Spectrometer. Microcalorimetry is a powerful technology for high-resolution X-ray spectroscopy that has been used in numerous experiments and has progressed steadily, with $\Delta E < 2$ eV achieved in recent laboratory tests. However, it has been a challenge to use this technology in arrays with good imaging capabilities. This is now changing. For *SMART-X*, we baseline the X-ray Microcalorimeter Imaging Spectrometer (XMIS) to provide high spectral resolution over a 0.2–10 keV band, as well as high angular resolution over a moderate field of view.

XMIS is a 300 × 300 array of 50 μm pitch pixels, uniformly covering a 5′ × 5′ ***field of view*** with 1″ ***spatial resolution***. While 90,000 appears to be a large number of pixels for microcalorimeters, the instrument we envision will be similar in cost and resources to that proposed for AXSIO. This assertion is based on current status and advances expected from existing and funded development programs over the next several years.

One cornerstone of our design is the use of position-sensitive microcalorimeters known as "Hydras", where a single Transition Edge Sensor (TES) is coupled to more than one discrete absorber (see Fig. 6 for a 3 × 3 Hydra). Each absorber element has a different thermal conductance to the sensor that results in position information being encoded in the pulse shape (Fig. 6b). This type of device has been successfully fabricated and tested in larger sizes for astrophysics and performs as predicted [17, 18]. Algorithms have been developed to identify X-ray events down to low energies, ~ 0.2 keV. Hydras with 16 absorbers per TES have been designed and are being tested, and Hydras with as many as 25 absorbers are considered possible. We estimate that < 5 eV ***energy resolution*** (FWHM, rms average within one Hydra) will be possible with 5 × 5 arrays of individual 50 mum absorbers. The maximum number of wire pairs between any two TESs is 15–19, which we estimate can be accommodated between absorbers in a planar geometry using the ~ 4 μm wire pitch stripline wiring already demonstrated in arrays designed for solar applications.

The estimated ***count rate capability*** is 20 cnt s^{-1} per TES for the 25-absorber Hydra. The resulting throughput is 0.8 cnt s^{-1} per 1″ pixel, sufficient to image all but the brightest known extended X-ray sources. For example, the brightest spots in Cas-A will still be under the saturation threshold. In the M87 field (Fig. 8d), only the AGN and the brightest knot in the jet will be saturated.

The current TRL of the XMIS subsystems (detector, read-out, focal-plane assembly, and the cryogenics) with respect to the *SMART-X* requirements range from 2–3 to 5, and ongoing technology development efforts will raise them to TRL5 for all these components by 2015–2017. For example, the use of current-steering multiplexing [19] has a 3-year program of ROSES-APRA technology development funding. With the speed necessary for the *SMART-X* TES design, we conservatively predict that the ability to multiplex 64–128 TESs per read-out channel will be demonstrated within three years. Combined with the use of 25 absorber Hydras, the number of required readout channels will be similar to that needed for the AXSIO XMS design (~ 68).

4 *SMART-X* Science

4.1 Meeting the RFI Requirements. Except for sensitivity at $E > 10$ keV and timing for 10^6 cnt s^{-1}, *SMART-X* meets or exceeds all requirements of the present RFI and addresses all of its major science questions:

What happens close to a black hole? Although the effective area at 6 keV is 0.17 m^2, a factor of 4 below IXO, *SMART-X* still will be able to measure motions of individual hot spots and test GR in 5–10 X-ray bright SMBHs through time-resolved Fe line spectroscopy.

When and how did SMBHs grow? Similarly, BH growth history can be constrained [20] through observations of the BH spin distribution in a sample of ~ 40 low-z SMBH (vs. 300 for IXO). For a handful of objects, the measurements can be done at z up to 3 (Fig. 7). Additional insights into the growth of SMBHs will be provided through studies of their first generations ($z > 6$) through surveys, for which *SMART-X* capabilities are unique (§4.5).

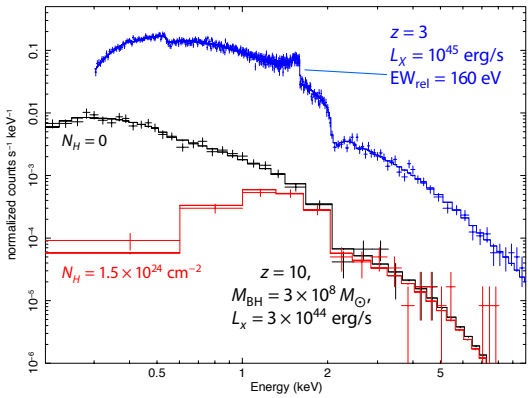

Fig. 7— 300 ksec *SMART-X*/APSI observation of a Sloan $z = 6$ quasar progenitor at $z = 10$. Growth at 10% Eddington rate has been assumed, resulting in $M_{BH} = 3 \times 10^8\ M_\odot$ and unobscured $L_X = 3 \times 10^{44}$ erg s^{-1} (2–10 keV). Such quasars are easily detectable even if highly obscured (*red*). *Blue:* 300 ksec XMIS observation of a "typical" eRosita AGN at $z = 3$ with a relativistically broadened Fe line (EW = 160 eV).

How does large scale structure evolve? The *SMART-X* sensitivity for weak absorption lines in the WHIM exceeds the RFI requirements by a factor of > 2 because of a higher throughput and resolving power [$\propto (AR)^{1/2}$]. *SMART-X* exceeds all requirements for measuring the growth of cosmic structure and evolution of the elements through observations of galaxy clusters to $z \sim 2$. A "precision cosmology" program [22] resulting in accurate structure growth measurements to $z \sim 1.5$ can be executed in < 10 Msec in combination with the weak lensing data from Euclid.

What is the connection between supermassive black hole formation and evolution of large scale structure? Cosmic feedback. We estimate that the baselined 5 eV energy resolution of XMIS will be sufficient for plasma line diagnostics and velocity structure measurements in the intracluster and interstellar media. With arcsecond angular resolution, detections of AGN feedback in clusters can be extended to $z \sim 1$, spatially-resolved velocity structure measurements can be done at $z \sim 0.5$ (Fig. 1). True 1″ spectro-imaging will illuminate the physics of AGN interactions with the cooling gas in the cluster cores through detailed measurements of the turbulence power spectrum and observations of flows near the hot/cold gas interfaces (Fig. 8b).

How does matter behave at very high density? CATGS throughput exceeds the RFI requirement by a factor of 4, correspondingly improving efficiency of the neutron star equation of state measurements.

SMART-X capabilities make it a versatile observatory with strong appeal to a very broad cross-section of the astronomical community. All areas of active X-ray astronom-

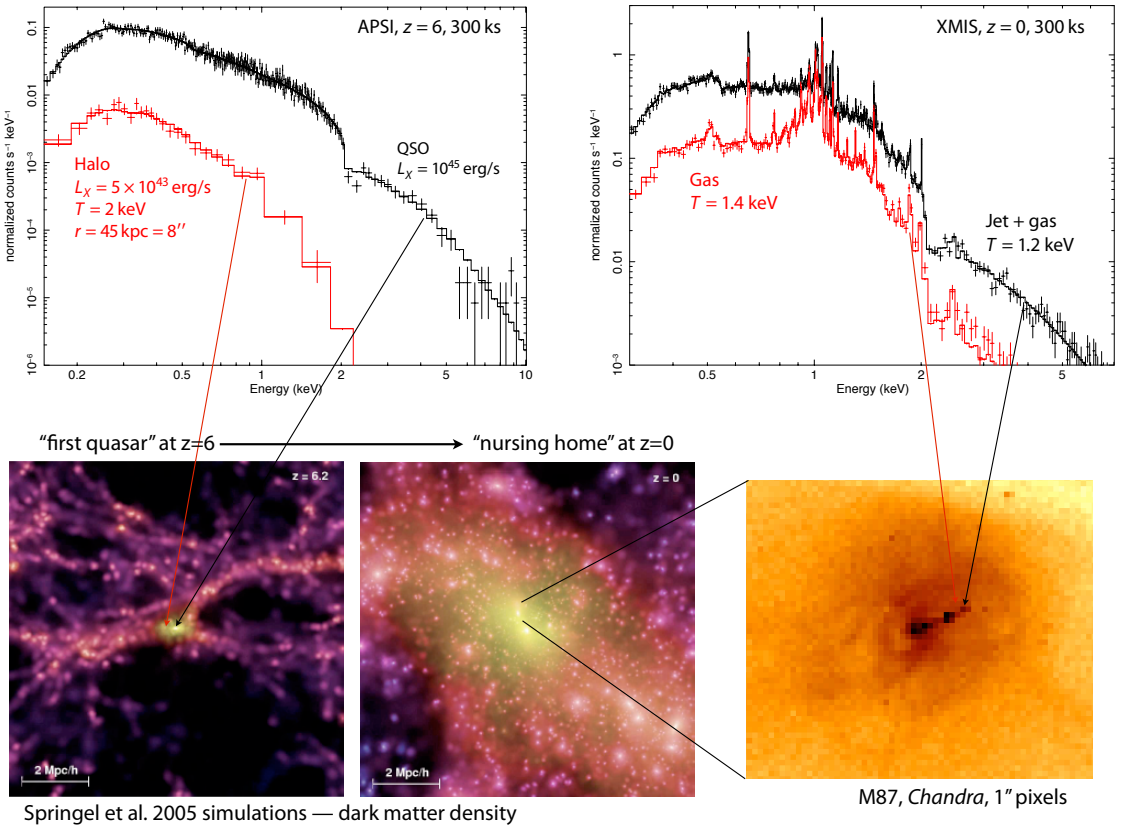

Fig. 8— *SMART-X* view of the environment of the "first quasars" and their descendants at $z = 0$. Sloan quasars must be located in the most massive halos existing at $z = 6$, $M = (2-6) \times 10^{12}\, M_\odot$ with $r_{\rm vir} \approx 50$ kpc [21]. These halos resemble cores of today's rich galaxy clusters both in terms of the dark matter density and X-ray properties [$T = 1.5-3$ keV, $L_X = (2-9) \times 10^{43}$ erg s^{-1}]. *SMART-X* will be able to separate this faint halo from the bright quasar emission *spatially* in a 300 ksec APSI observation. Descendants of the first quasars at $z = 0$ are at the centers of rich galaxy clusters. A 300 ksec observation of a low-z cluster core with XMIS yields enough counts for detailed spectroscopy in $1'' \times 1''$ regions.

ical research today — evolution of galaxy clusters and hierarchical structure growth; metal enrichment of the IGM reflecting the history of star formation; AGN feedback, duty cycles and relation between the radio- and quasar modes; source populations in nearby galaxies; physics of supernova remnants; etc. etc. — will reach new heights with *SMART-X*.

The high angular resolution emphasized in the *SMART-X* design enables science well beyond that considered by Astro2010 for IXO. It will open new windows for X-ray astronomy in studies of the high-z Universe, in the time domain, and in high-resolution spectroscopy. In the space remaining, we give only a few examples of what *SMART-X* would achieve for studies of galaxy formation and growth of supermassive black holes.

4.2 Supermassive black holes and their environment to z = 6 and beyond. Studies of the first generation of black holes and their host galaxies which by $z \approx 6$ have ionized nearly all of the hydrogen in the Universe is one of the major topics highlighted by Astro2010.

Quasars at $z \sim 6$, discovered in the SDSS and other surveys [23–25], are extremely luminous and massive, $M_{\rm BH} \sim 10^9\, M_\odot$ [24]. To form such a massive BH at high z is a great challenge for theory. Depending on the typical accretion rate, the progenitor masses at $z = 10$ range from $M_{\rm BH} \sim 3 \times 10^8\, M_\odot$ for $\dot{M} = 0.1 \dot{M}_{\rm Edd}$ to $\sim 7500\, M_\odot$ for an Eddington rate. Observations of this progenitor population are one of the best ways to solve the puzzle of the seed BH origin [26].

Many $z = 6$ quasars are detected in short *Chandra* observations to have $L_X \sim 10^{45}$ erg s^{-1} [27]. Assuming that $L_X \propto M_{BH}$, we expect $L_X \approx 3{\times}10^{44}$ erg s^{-1} for a $3{\times}10^8\, M_\odot$ SMBH at $z = 10$. *SMART-X* sensitivity is sufficient (Fig. 7) for spectroscopy of such quasars, even if they are highly obscured and thus undetectable in the optical or IR. In a medium-sensitivity survey observation, 100 ksec with APSI, a 10 photons detection threshold at $z = 10$ corresponds to a low-luminosity AGN, $L_X = 6.5 \times 10^{42}$ erg s^{-1} or $M_{BH} \approx 6.5 \times 10^6 M_\odot$. *SMART-X* will be able to survey ~ 10 deg^2 to this depth, so any significant population of such SMBH at $z = 10$ will be uncovered.

The growth of SMBH is intimately connected with the properties and environment of their host galaxies. *SMART-X* will be able to directly study the connection

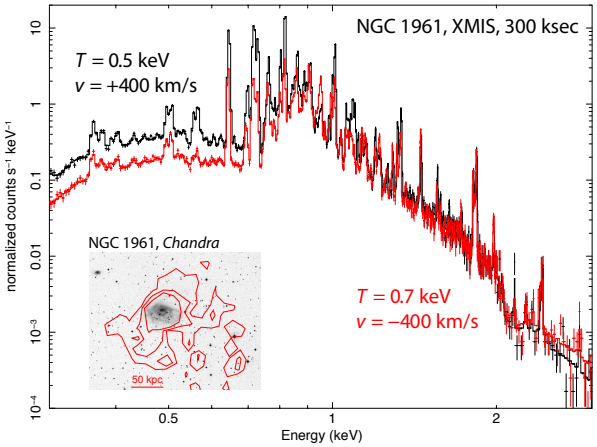

Fig. 9— Simulated 300 ksec *SMART-X*/XMIS observation of the hot gaseous corona around NGC 1961 [28]. The best-fit *Chandra* model was separated into two components with slightly different temperatures and bulk velocities expected in massive halos [29]. Temperatures, ionization states, and chemical abundances of different elements are easily derived from such spectra, and relative velocities can be measured to ± 30 km s^{-1}.

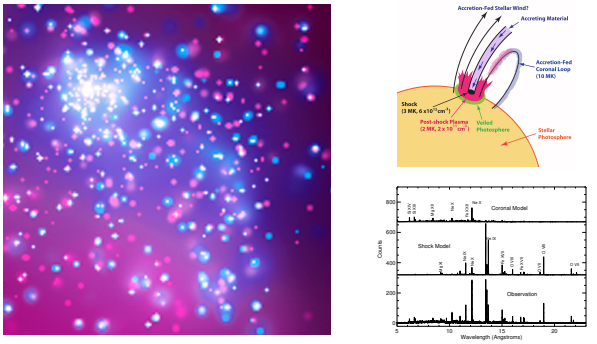

Fig. 10— *Left: Chandra* 60 ksec observation [38] of the Trumpler 14 complex in the Carina Complex ($5' \times 5'$ region) contains ~ 1000 stars down to $\log L_X \simeq 29.8$ erg s^{-1}. A similar single observation with *SMART-X*/XMIS will result in detection of ~ 10,000 stars and provide high-resolution spectra of a dozen OB stars and hundreds of flaring/active T Tauri stars. X-ray spectroscopy is a key diagnostics of the physics of coronae of active stars (*right*, from [39]).

to $z = 6$. Springel et al. [21] argue that the $M_{\rm BH} \sim 10^9\,M_\odot$ Sloan quasars must be located in the biggest galaxies and hence in the biggest dark matter halos existing at that epoch. These host halos resemble the cores of today's galaxy clusters both in their X-ray properties and dark matter density — $M_{\rm tot} = (2-6) \times 10^{12}\,h^{-1}\,M_\odot$, $r_{\rm vir} \approx 50$ kpc, $T = 1.5$–3 keV and $L_X = (2$–$9) \times 10^{43}$ erg s^{-1}. Although the halo X-ray emission is only a small fraction of the quasar's flux, and normally is undetectable, *SMART-X*, can easily separate the quasar and the halo *spatially* ($1''$ = 5.5 kpc at $z = 6$), and in a 300 ksec APSI observation halo's gas temperature will be measured (Fig. 8).

Through detailed *SMART-X* spectroscopy of quasars at $z \le 6$, we can detect powerful SMBH-driven winds [30], use Fe line to detect the presence of multiple SMBHs [31], and in some cases observe strong gravity effects (Fig. 7).

Fast-forwarding to $z = 0$, the SMBHs of the first quasars should lie at the centers of rich galaxy clusters [21], and many have switched to "radio-mode" (e.g., [32]). A moderately-deep XMIS observation (300 ksec) of a low-z cluster will provide an amazingly detailed picture of the "nursing home of the first quasar"; enough photons for detailed spectroscopy will be collected in individual $1'' \times 1''$ pixels (Fig. 8, right). Even at $z = 0.5$, *SMART-X* will be able to observe interactions of AGNs with the cluster gas with a remarkable level of detail (Fig. 1).

4.3 Galaxy and star formation. Galaxy formation is also highlighted in the Astro2010 report. Evolution of star formation in objects of different mass is now tracked to $z \lesssim 1$ in surveys such as COSMOS [33]. The results are puzzling in that > 70% of baryons in galaxy-sized halos are missing (e.g, [34]). Almost certainly, these baryons are expelled from the galaxy halos. Possible ejection mechanisms are energy feedback from the SMBH growth [35]; galactic winds driven by stellar feedback [36]; or self shock-heating of the infalling gas inside the halos with $M_{\rm tot} > 3 \times 10^{11}\,M_\odot$ [29]. Regardless of the exact mechanism, for the gas to leave a halo, a significant fraction of it must be heated to ~ the halo virial temperature, $T \gtrsim 0.3$ keV for large galaxies, making it observable only in the X-rays.

Stellar material in the galaxies is observed in the optical near-IR; molecular gas and dust deep inside the star-forming regions will be detected by ALMA and EVLA; cold hydrogen in the 100-kpc galaxy halos at high redshifts is observed in Ly-α [37]. The picture is incomplete without observations of the hot gas phase expected to contribute ~ ⅓ of the total baryonic mass. Thus X-ray data are essential to complete the observational picture of galaxy assembly. As we discuss below, the hot gas should be detectable with SMART-X around massive star-forming galaxies in a wide range of redshifts reaching to $z = 2.5$.

To estimate the detectability of hot gas halos at high redshifts with *SMART-X*, we consider kinematic studies of Ly-α selected galaxies at $z \approx 2.5$ [42]. These are active, star-forming galaxies (SFR $\approx 30\,M_\odot$ yr^{-1} [43]), whose halos ($M_{\rm tot} \sim 9 \times 10^{11}\,M_\odot$) contain on average $7 \times 10^{10}\,M_\odot$ of cold gas with bulk velocities 500 – 800km s^{-1}. Collisions of individual gas clouds at such velocities should heat a fraction of the halo baryons to $T \sim 1$ keV. Assuming that the mass of hot and cold gas phases within the halo is similar (as in NGC 1961, see below), one expects X-ray luminosities of 3×10^{42} erg s^{-1} in a diffuse component extending to ~ 80 kpc = $10''$. A 300 ksec observation of such an object with *SMART-X*/APSI will yield 500 photons, enough to measure the temperature, density, and overall morphology of the gas halo. The halo will be easily separated spatially from the X-ray flux of discrete sources within a compact star-forming region of the galaxy.

Less speculative are the prospects for detailed observations of circumgalactic gas around low-z spirals because several detections have already been made with *Chandra*.

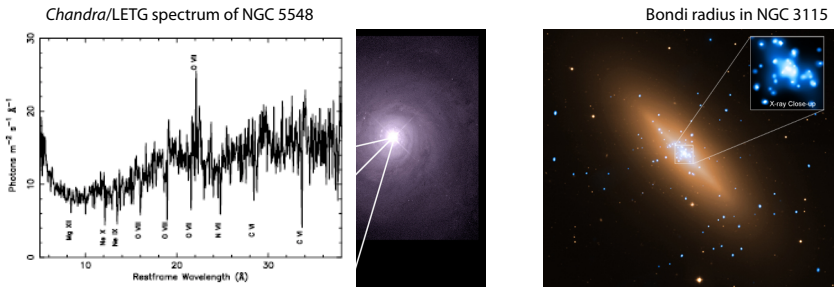

Fig. 11— *Left: Chandra*/LETG observation of an outflow in the vicinity of the AGN in NGC 5548 [40]. *Right:* Estimated Bondi radius in NGC 3115 is 4″ with FWHM of the central emission peak ≈ 3″ [41]. *SMART-X*/CATGS energy resolution for such sources will be $R > 1000$, while providing 0.5″ angular resolution across the dispersion direction.

Examples include well-known observations of galaxy-scale winds in M82, and a recent detection of a 50 kpc-scale diffuse halo in NGC 1961 [28]. The NGC 1961 halo has an X-ray luminosity of 4×10^{40} erg s^{-1} and temperature of 0.6 keV, and is estimated to contain $5 \times 10^9\ M_\odot$ of hot gas within 50 kpc and $2 \times 10^{11}\ M_\odot$ within the virial radius, roughly the stellar mass in the system and 4× the mass of the cold gas. Such a halo observed for 300 ksec with *SMART-X*/XMIS would provide a uniquely informative measurement of the thermal, chemical, and kinematic structure of the hot gas (Fig. 9).

To complete the X-ray view of cosmic star formation, *SMART-X* will be able to look deep inside star forming regions in the Milky Way (Fig. 10), and study processes ranging from the physics of protoplanetary disks [39, 44] to elemental abundance, shocks, absorption and charge-exchange emission in the surrounding ISM.

4.4 High-resolution spectroscopy. The combination of *SMART-X* mirrors with the CAT transmission gratings will provide immensely powerful spectroscopic capabilities in the soft X-ray band. Absorption line observations of the gas outflows around AGNs [40, 45] will be routine, and measurements of the neutron star equation of state [46] feasible. The new aspect of CATGS is that it is highly dispersive and will provide $R = 1000$ resolving power even for sources with a size of 3″ − 5″, while the 0.5″ spatial resolution will be available across the dispersion direction. Therefore, CATGS will be able to make detailed spectro-imaging observations of slightly extended objects such as the emission from within the Bondi radius in NGC 3115 ($r = 4''$, $T \approx 0.5$ keV [41], Fig. 11b).

4.5 Surveys. *SMART-X* can carry out surveys matching the scope of the future deep optical, IR, and mm/submm surveys. Its instrumental background is close to *Chandra*'s because of the same focal length and similar orbit, $\approx 10^{-6}$ cnt arcsec^{-2} s^{-1}. If we consider detections in the 0.7–2 keV band where the Galactic foreground contamination is low [47], then for typical power law spectra, *SMART-X*/APSI has a factor of ∼ 50 higher throughput than *Chandra*/ACIS-I — a combined gain of factors of 30 and 1.6 due to the mirror area and soft-band QE of APSI, respectively. Therefore, the sensitivity limit of the 4 Msec *Chandra* Deep Field South will be reached with *SMART-X* in 80 ksec. Sensitivity will be fully photon-limited because even at 10′ off-axis where the PSF is 4″ HPD, there will be only 1 background event per resolution element at this exposure. The *Chandra* PSF degrades to 4″ HPD at 7′ off-axis, so *SMART-X* provides not only a higher sensitivity but also a wider FOV. The grasp of *SMART-X* is a factor of 98 higher than *Chandra's*. A 10 deg^2 survey to the CDFS depth can be carried out in 8.1 Msec. A 4 Msec individual pointing will reach on-axis sensitivity (for 10 cnt detections) of 3.0×10^{-19} erg s^{-1} cm^{-2} in the 0.5–2 keV band, corresponding to $L_X^{(2-10)} = 3.3 \times 10^{41}$ erg s^{-1} at $z = 10$.

4.6 Time-domain X-ray astronomy. With *SMART-X* operating in the 2020's and potentially beyond, there will be a sufficient time span relative to *Chandra* to observe secular evolution in a number of astronomical objects, thus opening a completely new window for X-ray astronomy. Examples include the evolution of the compact object and shocked plasma in Cas-A and other young supernova remnants (Δt/age ∼ 10%) and the spectacular fireworks display in SN1987A expected over the next few decades as increasing amounts of metal-rich ejecta are lit up by the reverse shock. Past activity of the Milky Way's central black hole can be tracked by evolution of its light echos on the molecular clouds around Sgr A*. Repeated 100 ksec observations of a single field ∼ twice a year over a 5 years span will provide a detailed picture of variability for 100's of high-redshift AGNs.

5 *SMART-X* Mission

We envision the launch of *SMART-X* to a 700,000 km orbit about the L2 point. The total mass of the *SMART-X* payload is 2863,kg (this includes an estimated mass, 1300 kg, of the spacecraft with the optical bench). With a 30% growth contingency and 200 kg propellant, the total "wet" mass is 3922 kg. This is comfortably launchable with Atlas V-541 (> 5000 kg throw mass).

The mission design and operations share great similarities to both *Chandra* and AXSIO. Compared to *Chandra*, *SMART-X* has a slightly lower (17%) overall mass, while the telescope assembly mass is 28% less. Key requirements — including alignment, stability, pointing control and aspect determination — will be essentially the same, and therefore require no new technology. The main difference

is higher peak science data rates, and increased power requirements for thermal control of the optics and operating XMIS. Compared to AXSIO, *SMART-X* will share the same general layout, but with an updated optic, a second focal plane instrument, and a translation stage, resulting in ≈30% larger mass and power requirements. Much of the *Chandra* ground software for all aspects of operations and science can be reused for *SMART-X*.

5.1 Cost. The major new technology development required to realize the *SMART-X* mission is the adjustable optics to provide the large area, low mass, 0.5″ resolution telescope at an affordable price. The cost of this program is estimated at $45M in the next 6–8 yr (see p.4 and Appendix B) — a rather modest investment to achieve the gains possible with *SMART-X*. An additional technology investment of ~ $30M is required to bring the science instruments to TRL 5/6.

Even though the SMART-X concept is new and has not been evaluated by the MDL, much of the work done for AXSIO is directly relevant, as is the *Chandra* experience. We can start with the detailed assessment done by the AXSIO team and the MDL and then identify differences for *SMART-X*. The summary is given in Table 2 and the cost methodology follows.

Flight Mirror Assembly Overall, we estimate the total ***added cost for the* SMART-X *mirrors to be at $170M, including 50% reserves.*** It includes doubling the AXSIO cost ($54M) for mandrels — while essentially the same number of mandrel pairs is required (*SMART-X* has more shells but a single mandrel can be used for up to 3 adjacent shells because the optics are adjustable), the mandrels require better upper-mid frequency figure and the mandrels have larger area. The cost of AXSIO module facilities ($30M) is scaled by a factor of 2 to account for the greater accuracy required, and then by the number of modules (42 vs. 60 for AXSIO), resulting in a net increase of $12M. The AXSIO cost of mirror manufacture ($174M) is increased by 5% or $8.7M to account for additional metrology time (estimated at 1 hour per mirror) to calibrate the PZT adjuster influence functions for each segment. Note that the total number of mirror segments is similar, 8256 for AXSIO vs. 8016 for *SMART-X*, which essentially eliminates any other impacts for the larger aperture.

These components add $75M to the cost of production of AXSIO mirrors, $282M, leading to a total of $357M for *SMART-X*. Given the novelty of the *SMART-X* mirror technology, we believe it is prudent to allow for 50% reserves, resulting in $536M, an overall increase of $170M relative when we include 30% reserves carried by AXSIO.

Science instruments and other differences. *SMART-X* introduces an additional science instrument, APSI. The CATGSR array, using identical technology, replaces the CCD-based readout array for AXSIO/XGS ($35M). Taking into account a streamlined configuration of the CATGS readout, we estimate the cost of APSI +CATGSR as double that of the AXSIO/XGS readout, an additional $35M.

Table 2— Resource and cost comparison of *SMART-X* and AXSIO

	SMART-X		Δ from AXSIO		
	m, kg	*P*, W	*m*, kg	*P*, W	Cost[1]
Mirrors	890	1000	418	650	**$170M**
Science instruments & spacecraft systems					**$188M**
APSI +CATGSR	107	300	65	250	
XMIS	358	1100	0	0	
Gratings	64	0	52	0	
Translation stage	144	0	144	0	
Integration & Test					**$52M**
Atlas V-541 launch					**$20M**
Total[2]	**2863**	**2817**			

[1] All added costs include reserves, as explained in the text. [2] Total mass and power also include spacecraft systems.

To achieve 4000 cm^2 gratings effective area, CAT gratings facets need to cover a factor of 5.3 larger aperture area compared to AXSIO/XGS. Scaling the AXSIO/XGS fabrication cost ($15M) by the area, we estimate an added cost of $65M for *SMART-X*.

We assume no additional costs for the XMIS. The translation table cost is estimated at $37M from the *Chandra* cost; an extra $3.7M is required for larger solar panels, and $4M for upgraded aspect cameras.

The added cost of the science instruments and upgrades to the spacecraft systems is thus $144.7M, ***or $188M including 30% reserve.***

To account for the extra complexity of X-ray test facilities and testing efforts, we double the AXSIO cost ($52M, including 30% reserve). Finally, the cost of launch with Atlas V-541 is $20M higher than that with 521 for AXSIO.

Adding all these extra components to an estimated end-to-end cost of the AXSIO mission, $1,898M, we obtain a ***total end-to-end mission cost of $2,328M for* SMART-X.**

Testing vs.* Chandra *cost. We can independently cross-check the above cost estimates against the actual cost of building *Chandra*, $2,521M in FY2012 dollars. This should be compared against the estimated cost of *SMART-X* excluding launch, ground system, and post-launch operations — $1,838M, obtained by adding *SMART-X* extras to the corresponding cost of AXSIO. The inflated *Chandra* cost is most certainly an overestimate because it is based on labor rates while parts and components have escalated less. Also, technology investments already made as well as the *Chandra* knowledge base and experience are significant savings factors for *SMART-X* (e.g., optics metrology is in hand for *SMART-X* but had to be developed for *Chandra*).

The *SMART-X* mission concept for a 2.3 m^2, 0.5″ resolution X-ray telescope, with 5′ FOV, 1″ pixel size microcalorimeter, 22′ FOV imager, and high-througput gratings, is challenging. However, we will be working with known requirements and capabilities, once the mirror technology is proven. The science will be extraordinary.

References

[1] Alcock, S., 2011, in *4th Workshop on Adaption and Active X-ray and XUV Optics*, http://www.diamond.ac.uk/Home/actop/programme.html
[2] Shine, R.A. et al., 2010, AGU Fall Meeting
[3] Rowlands, N. et al., 2004, SPIE Proc., 5487, 646
[4] Wolf, R. A. & Troiler-McKinstry, S., 2004, J. Appl. Phys., 95, 1397
[5] Shepard, J. F. Jr. et al., 1999, J. Appl. Phys., 85, 6711
[6] Troiler-McKinstry, S., 2011, private communication
[7] Davis, W., Reid, P. B. & Schwartz, D. A., 2010, SPIE Proc., 7803, 78030P
[8] Schwartz, D. A. et al., 2011 (SPIE), vol. 8147
[9] Luo, L. et al., 2007, Appl. Phys. Lett., 90, 102907
[10] Lehan, J. et al., 2005, SPIE Proc., 5900, 59001D
[11] Lee, S. C. et al., 1992, IEEE Trans. Nucl. Sc., 39, 2036
[12] Heilmann, R. K. et al., 2010, in M. Arnaud, S. S. Murray & T. Takahashi, eds., *in Space Telescopes and Instrumentation 2010: Ultraviolet to Gamma Ray*, vol. 7732, 77321J
[13] Falcone, A. D. et al., 2007, in *Society of Photo-Optical Instrumentation Engineers (SPIE) Conference Series*, *Society of Photo-Optical Instrumentation Engineers (SPIE) Conference Series*, vol. 6686
[14] Suntharalingam, V. et al., 2007, in *Society of Photo-Optical Instrumentation Engineers (SPIE) Conference Series*, *Society of Photo-Optical Instrumentation Engineers (SPIE) Conference Series*, vol. 6690
[15] Janesick, J. et al., 2007, in *Society of Photo-Optical Instrumentation Engineers (SPIE) Conference Series*, *Society of Photo-Optical Instrumentation Engineers (SPIE) Conference Series*, vol. 6690
[16] Lechner, P. et al., 2010, in *Society of Photo-Optical Instrumentation Engineers (SPIE) Conference Series*, *Society of Photo-Optical Instrumentation Engineers (SPIE) Conference Series*, vol. 7742
[17] Smith, S.J. et al., 2009, IEEE Transactions on Applied Superconductivity, 19, no. 3, 451
[18] Smith, S.J. et al., 2008, Proc. SPIE, 7011, 701126
[19] Irwin, K.D. et al., 2011, arXiv:1110.1608
[20] Brenneman, L. et al., 2009, in *astro2010: The Astronomy and Astrophysics Decadal Survey*, *Astronomy*, vol. 2010, 26–+
[21] Springel, V. et al., 2005, Nature, 435, 629, millenium simulation
[22] Vikhlinin, A. et al., 2009, in *astro2010: The Astronomy and Astrophysics Decadal Survey*, *Astronomy*, vol. 2010, 304–+
[23] Fan, X. et al., 2006, The Astronomical Journal, 132, no. 1, 117
[24] Willott, C. J. et al., 2010, The Astronomical Journal, 140, no. 2, 546
[25] Mortlock, D. J. et al., 2011, Nature, 474, 616
[26] Volonteri, M., 2010, A&A Rev., 18, 279
[27] Shemmer, O. et al., 2006, The Astrophysical Journal, 644, no. 1, 86
[28] Anderson, M. E. & Bregman, J. N., 2011, The Astrophysical Journal, 737, no. 1, 22
[29] Kereš, D. et al., 2009, Monthly Notices of the Royal Astronomical Society, 395, no. 1, 160
[30] Chartas, G. et al., 2009, ApJ, 706, 644
[31] Li, Y. et al., 2007, ApJ, 665, 187
[32] Merloni, A. & Heinz, S., 2008, MNRAS, 388, 1011
[33] Leauthaud, A. et al., 2011, ArXiv e-prints
[34] McGaugh, S. S. et al., 2010, The Astrophysical Journal Letters, 708, no. 1, L14
[35] Croton, D. J. et al., 2006, Monthly Notices of the Royal Astronomical Society, 365, 11
[36] Governato, F. et al., 2010, Nature, 463, 203
[37] Matsuda, Y. et al., 2011, Monthly Notices of the Royal Astronomical Society: Letters, 410, no. 1, L13
[38] Broos, P. S. et al., 2011, ApJS, 194, 2
[39] Brickhouse, N. S. et al., 2010, ApJ, 710, 1835
[40] Kaastra, J. S. et al., 2000, Astronomy and Astrophysics, 354, L83
[41] Wong, K.-W. et al., 2011, The Astrophysical Journal Letters, 736, no. 1, L23
[42] Steidel, C. C. et al., 2010, The Astrophysical Journal, 717, no. 1, 289
[43] Erb, D. K. et al., 2006, The Astrophysical Journal, 647, no. 1, 128
[44] Feigelson, E. D., 2010, Proceedings of the National Academy of Science, 107, 7153
[45] Kaspi, S. et al., 2002, The Astrophysical Journal, 574, no. 2, 643
[46] Paerels, F. et al., 2009, in *astro2010: The Astronomy and Astrophysics Decadal Survey*, *Astronomy*, vol. 2010, 230–+
[47] Markevitch, M. et al., 2003, The Astrophysical Journal, 583, no. 1, 70

A List of Acronyms

ACIS — Advanced CCD Imaging Spectrometer

AGN — Active Galactic Nucleus

AIA — Atmospheric Imaging Assembly

APSI — Active Pixel Sensor Imager

AXSIO — Advanced X-ray Spectroscopic Imaging Observatory

BH — Black Hole

CATGS — Critical Angle Transmission Grating Spectrometer

CATGSR — Critical Angle Transmission Grating Spectrometer Readout

CDFS — Chandra Deep Field - South

CDM — Code Division Multiplexing

CMOS — Complemetary Metal Oxide Semiconductor

DEPFET — Depleted p-channel Field Effect Transistor

EPE — Extreme Physics Explorer

EW — Equivalent Width

FEM — Finite Element Model.

FPA — Focal Plane Assembly

HETG — High Energy Transmission Grating

HPD — Half Power Diameter

IGM — Intergalactic Medium

IXO — International X-ray Observatory

LETG — Low Energy Transmission Grating

MDL — Mission Design Lab

PZT — Lead Zirconate Titanate

SFR — Star Formation Rate

SMBH — Supermassive Black Hole

TES — Transition Edge Sensor

TRL — Technology Readiness Level

WHIM — Warm-hot intergalactic medium.

XMIS — X-ray Microcalorimeter Imaging Spectrometer

B Optics Development Plan

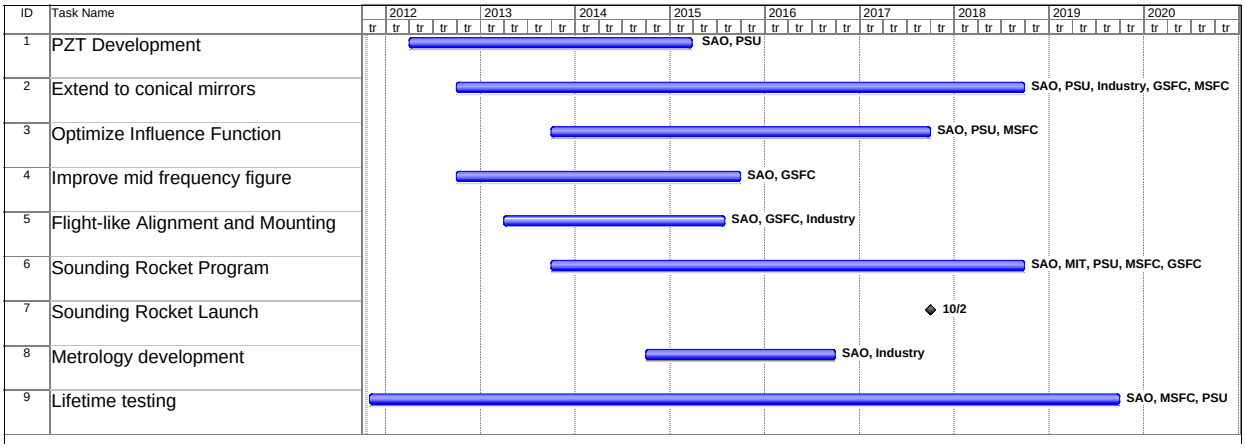

Previous funding includes NASA contracts NNG04GK28G; NNX08AT62G; NASA Contract NNX09AE87G, SAO internal funding, and a grant from the Gordon & Betty Moore Foundation.

C Current TRL Assessment for XMIS

A microcalorimeter instrument consists of 4 main components - the detector, read-out, focal-plane assembly (FPA), and the cryogenics. Each of these components can be broken down further. Here we briefly summarize these technical readiness levels in the context of the requirements for *SMART-X*. The number of amplifier read-out channels is similar to IXO, so we can draw from the wealth of knowledge gained from studies of this mission.

Detector: Hydras with 50 micron pitch absorbers, fabricated on a solid substrate, and going up to numbers of 16-25 have not yet been demonstrated. The Hydra concept is generally well understood, and the example designs that have so far been fabricated have performance that match well to the expectations, similar to simple single-pixel devices. Single-pixel devices roughly of the size and design needed for *SMART-X* have also shown the expected performance. The program to develop microcalorimeters for solar applications is researching 3×3 Hydras of this small absorber size scale. Therefore, the TRL can be safely assessed at 2–3. Leveraging these advances, we predict that the TRL will be at TRL5 for 32×32 arrays of 3×3 Hydra arrays in 2013. For 4×4 or 5×5 Hydras, and increasing array sizes to 60×60 TESs, we would need new technology funding to develop these devices. With support, TRL5 for these requirements can be met in the 2015–2017 time-frame.

Readout: Although the IXO read-out was assigned a technology readiness level of 4–5, the requirements for *SMART-X* have lead to the proposed use of current-steering code division multiplexing (I-CDM), which is at the TRL ~ 3. However, because of its similarity to time division multiplexing, we expect that the technology readiness level will advance quickly to TRL5 by 2014 under a newly funded NASA ROSES program.

FPA: While the Astro-H FPA is currently at TRL8, just as for AXSIO, the XMIS instrument will require a different design. Thus the FPA is assigned a TRL of 3–4. What is required for a higher level is some investment in support technology development, but there do not appear to be any major technical hurdles.

Cryogenics The technology readiness level for the cryogenics is already at an advanced stage due to the development of the Astro-H cryogenics, which, in its current form, will be the baseline for the EPE instrument. The cryocooler system and the adiabatic demagnetization refrigerator are currently at TRL5 and will be at TRL6 in 2012.